

# Chapter 2

## Lattice Methods for Hadron Spectroscopy

Sinéad M. Ryan

**Abstract** Lattice hadron spectroscopy is crucial to inform and direct a new generation of experiments. Useful calculations require control of both statistical and systematic uncertainties. In these lectures selected methods for lattice hadron spectroscopy are discussed in detail. The lectures aim to describe all aspects of a calculation from quark propagation to fitting and interpreting data. After some motivation for lattice spectroscopy, the path integral approach and construction of correlation functions are discussed. There are detailed discussions of techniques for quark propagators, including new developments in calculations of all-to-all propagators. Lattice and continuum symmetries are contrasted and techniques for spin identification in lattice calculations are discussed in some detail. Design and construction of optimal operators as well as fitting and systematic errors are addressed. Finally, open problems and challenges are described focusing on resonances and scattering states.

### 2.1 Introduction

The nonperturbative spectrum of mesons and baryons built from light and heavy quarks provides a fascinating arena in which to study the strong interaction. Indeed many of the most recently discovered hadrons have unexpected properties and their discovery has reignited theoretical and phenomenological interest in spectroscopy. Within the Standard Model (SM), to separate electroweak physics from strong-interaction effects we must first understand the hadron spectrum. Meanwhile beyond the SM, models of electroweak symmetry breaking, such as technicolour, may require nonperturbative techniques at the TeV scale which are similar to the techniques developed for spectroscopy at GeV scales. To understand therefore the new puzzling states which have been observed and to probe the physics at LHC energies better techniques for spectroscopy will be crucial and will help us to understand the nature of masses and transitions.

---

S.M. Ryan (✉)  
School of Mathematics, Trinity College, Dublin 2, Ireland  
e-mail: [ryan@maths.tcd.ie](mailto:ryan@maths.tcd.ie)

While the quark model has provided a useful framework in which to understand the structure of mesons and baryons it is limited to just a subset of the states which QCD in principle allows. Lattice QCD offers the prospect of nonperturbative, systematically-improvable model-independent calculations of hadron masses and mixing (as well of course as a wealth of other properties of QCD). In these lectures we will review some approaches and discuss new methods to address the significant challenges which remain in the era of dynamical calculations at realistic quark masses.

### 2.1.1 Notation and Basics

The objects of interest are formed from constituent quarks and antiquarks to make bound states of mesons and baryons as well as molecular and multi-quark states, hybrid states and glueballs. In QCD the fundamental constituents are the quarks (in six flavours) and gluons. The fields of the lagrangian are combined in colourless combinations forming bound states.

The quark model is a useful classification of hadrons in terms of their valence quarks—the quarks ( $q$ ) and antiquarks ( $\bar{q}$ ) that give the quantum numbers of the hadrons. States in the continuum are classified by the quantum numbers:  $J$ , the total angular momentum;  $P$ , the parity and  $C$ , charge conjugation. Recall that  $|L - S| \leq J \leq |L + S|$  and in the quark model naming scheme,  $n^{2S+1}L_J$ , the values of  $L$  are  $L = \{0, 1, \dots\}$  and  $S = \{0, 1\}$ . The parity is defined by  $P = (-1)^{(L+1)}$  and charge conjugation is  $C = (-1)^{(L+S)}$ . The latter is a good quantum number for  $q\bar{q}$  states with the same quark and antiquark flavour e.g. charmonium but not for example for heavy-light mesons,  $D_{(s)}$ ,  $B_{(s)}$ , nor for baryons.

#### 2.1.1.1 Mesons

Mesonic states are composed of two spin-half fermions, and described by  $^{2S+1}L_J$  in quark model notation with  $S = 0$  for antiparallel quark spins and  $S = 1$  when the quark spins are parallel.

States in the quark model follow a “natural spin-parity” series with  $P = (-1)^J$  and so have  $S = 1$  and thus  $CP = +1$ . With these conditions, the allowed states have  $J^{PC} = 0^{-+}, 0^{++}, 1^{--}, 1^{+-}, 2^{--}, 2^{-+}, \dots$ . However, states with  $P = (-1)^J$  but  $CP = -1$  are forbidden in a  $q\bar{q}$  model of mesons, meaning that the states  $J^{PC} = 0^{+-}, 0^{--}, 1^{-+}, 2^{+-}, 3^{-+}, (\text{even})^{+-}, (\text{odd})^{-+}, \dots$  which are allowed by QCD cannot be accommodated in a simple quark model picture and must therefore be more than a simple bound state of a quark and antiquark. These are the “exotic” states of QCD.

### 2.1.1.2 Baryons

In this case there are three quarks in colourless combination (with baryon number  $B = 1$ ),  $J$  is half-integer and in particular  $C$  is not a good quantum number so that states are classified by  $J^P$ . The spin-statistics theorem tells us that a baryon wavefunction must be antisymmetric under the exchange of any two quarks. Since all hadrons are colour neutral, the combinations of colour indices of the three quarks must be antisymmetric and the remaining labels: flavour, spin and spatial structure must be in totally symmetric combinations,

$$|qqq\rangle_A = |\text{colour}\rangle_A \otimes |\text{space, spin, flavour}\rangle_S. \quad (2.1)$$

The possible states are then

$$|qqq\rangle_A = |\text{colour}\rangle_A \otimes \frac{[|\text{space}\rangle_S \otimes |\text{spin}\rangle_A \otimes |\text{flavour}\rangle_A]_S}{[|\text{space}\rangle_S \otimes |\text{spin}\rangle_S \otimes |\text{flavour}\rangle_S]_S} \quad (2.2)$$

and a linear combination

$$|qqq\rangle_A = \alpha |\text{colour}\rangle_A \otimes [|\text{space}\rangle_S \otimes |\text{spin}\rangle_A \otimes |\text{flavour}\rangle_A]_S \\ + \beta |\text{colour}\rangle_A \otimes [|\text{space}\rangle_S \otimes |\text{spin}\rangle_S \otimes |\text{flavour}\rangle_S]_S.$$

with  $\alpha^2 + \beta^2 = 1$ . An outstanding question in baryon spectroscopy is that of missing states. For three quarks ( $u, d, s$ ) there is an (approximate)  $SU(3)$  flavour symmetry and a decomposition in flavour given by

$$3 \otimes 3 \otimes 3 = 10_S \oplus 8_M \oplus 8_M \oplus 1_A, \quad (2.3)$$

where  $A$  is antisymmetric,  $S$  is symmetric and  $M$  is mixed. The decuplet is symmetric in flavour and the two octets have a mixed symmetry and since they are related by a unitary transformation describe the same states. This analysis predicts many more states than observed by experiments, a phenomenon known as the missing resonance problem.

### 2.1.1.3 Gluonic Excitations: Hybrids and Glueballs

In addition to the mesons and baryons discussed above in terms of quark degrees of freedom, QCD allows for a richer spectrum of states when we take into account the gluonic degrees of freedom. We can formulate color-neutral states of pure glue, called glueballs and states in which excitations of the gluonic field in a hadron form so-called hybrids.

Theoretical discussions of glueballs focus on states made from two or three gluons and as for the conventional mesons and baryons these states are color neutral and have integer angular momentum. The two-gluon states will have  $J = 0$  (scalar or pseudo-scalar) or  $J = 2$  (tensor). Three-gluon states can have  $J = 1$  (vector) or  $J = 3$ .

Glueballs will mix with ordinary mesons and are therefore difficult to identify unambiguously in experiments. There is a considerable history of lattice calculations of glueballs. A pioneering quenched calculation mapped the spectrum of states in great detail [77]. However, unquenched calculations must also take into account the allowed mixing with ordinary mesons and are consequently more technically challenging. See for example [78] and references therein.

### ***2.1.2 Current and Future Experiments***

Before we delve into the details of lattice hadron spectrum calculations it is worthwhile to review briefly some of the experimental activity underway. There is significant new effort being devoted to understanding the light and charm spectra and to answering the questions:

1. Are there resonances that do not fit the quark model?
2. Are there gluonic excitations in these spectra?
3. What structure does confinement lead to?

#### **2.1.2.1 Current Status**

Since the early 2000s there has been a renaissance in charmonium spectroscopy. The unexpected discovery of new narrow structures above the open charm threshold by Belle and Babar led to substantial renewed interest in what was believed to be a well-understood sector. There has been much speculation about the nature of the so-called “X,Y,Z” states including possible molecular and hybrid states. Intriguingly the  $Z^\pm(4430)$  is a charged state and so cannot be a simple  $c\bar{c}$  meson. However, very little is definitively known and as yet no clear picture has emerged. BESIII continues to take data, with an aim to accumulate  $10^8$  to  $10^9$   $J/\Psi$  and  $\Psi'$  decays. These states decay primarily by  $c\bar{c}$  annihilation and hadronisation to light mesons. The experiment has reported new states including the  $X(1835)$ ,  $X(2120)$  and  $X(2370)$  [79]. However, no quantum number assignments have been made yet and both independent confirmation and measurement of the quantum numbers is essential.

### 2.1.2.2 Planned Experiments

The GlueX experiment at the Hall D facility at JLab plans to have first physics results in 2015. The primary goal is the search for and study of gluonic excitations in the meson spectrum, produced in  $\gamma p$  collisions. Photoproduction of exotic hybrids is expected to be particularly effective, while also allowing an extensive study of the conventional spectrum. As well as discovery, GlueX should in principle be able to confirm the existence of new states seen at BESIII, through a complementary production mode and in addition measure or confirm the measurement of quantum numbers. Using their proposed kaon identification system GlueX will additionally be able to study baryons, including excited  $\Xi$  baryons.

The PANDA experiment at the Facility for Antiproton and Ion Research (FAIR) which is under construction at GSI in Darmstadt will collide antiprotons with a fixed target. The hadron spectroscopy program at PANDA includes a search for gluonic excitations: glueballs and hybrids and charmonium spectroscopy: in particular of states above threshold. The goal is to find the missing  $D$  and  $F$  wave states in charmonium and to understand the nature of the  $X, Y, Z$  states. PANDA will also study the  $D$  meson spectrum, again to address the question of unexplained states which do not fit into the quark model picture for heavy-light systems. A comprehensive programme of baryon spectroscopy is also planned—in particular for strange and charmed baryons.

In principle, lattice QCD can provide a complementary approach as well discriminating between models and providing guidance for experimental searches to address these questions by identifying properties of states in the continuum limit of the theory and by going beyond precision ground state spectroscopy to compute scattering and resonance widths. To achieve this we need new tools: techniques for statistical precision, even at high spin; methods for operator construction and spin identification on the lattice; new methods for resonance and isoscalar physics; control of the relevant extrapolations ( $m_q \rightarrow m_{\text{physical}}, V \rightarrow \infty, a \rightarrow 0$ ). A discussion of recent progress to address some of these issues will be the main topic of these lectures. The topics I cover are not exhaustive but will I hope give a flavour of the progress being made, what you might expect to see in the near future and how to judge the relative merits of such calculations. There are many excellent textbooks, reviews and lecture notes available including this not exhaustive list [3, 5, 6, 21, 80–86].

### 2.1.3 Lattice Hadron Spectroscopy

An important goal for lattice calculations is a determination of the low-energy spectrum of quarks and gluons from the QCD Lagrangian

$$\mathcal{L}_{\text{QCD}} = -\frac{1}{4} F_{\mu\nu}^a F^{a\mu\nu} + \sum_f \bar{\Psi}_f (i \gamma^\mu D_\mu - m_f) \Psi_f, \quad (2.4)$$

where the index  $f$  represents flavour and the covariant derivative  $D_\mu$  is defined

$$D_\mu = \partial_\mu - ig \left( \frac{1}{2} \lambda^a \right) A_\mu^a. \quad (2.5)$$

In such calculations there are just two input parameters, the coupling  $g$  and the bare mass  $m_f$ . The continuum theory is recovered by simulating at or extrapolating to physical values of the light quark masses and in the limits  $a \rightarrow 0$  and  $V \rightarrow \infty$ .

At the Lattice conference in 2011, Hoelbling [87] reviewed progress in lattice spectroscopy, described in Fig. 2.1. The plots show that many lattice collaborations are now making simulations with  $N_f \geq 2$ , at light quark masses and large volumes. In these lectures I will not discuss fermion discretisations, chiral extrapolations or the details of simulations at or close to the physical point. Note that recent results for the low-lying spectrum of hadrons in the light sector show internal consistency between different lattice fermion formulations and impressive agreement with experimental results [88–92].

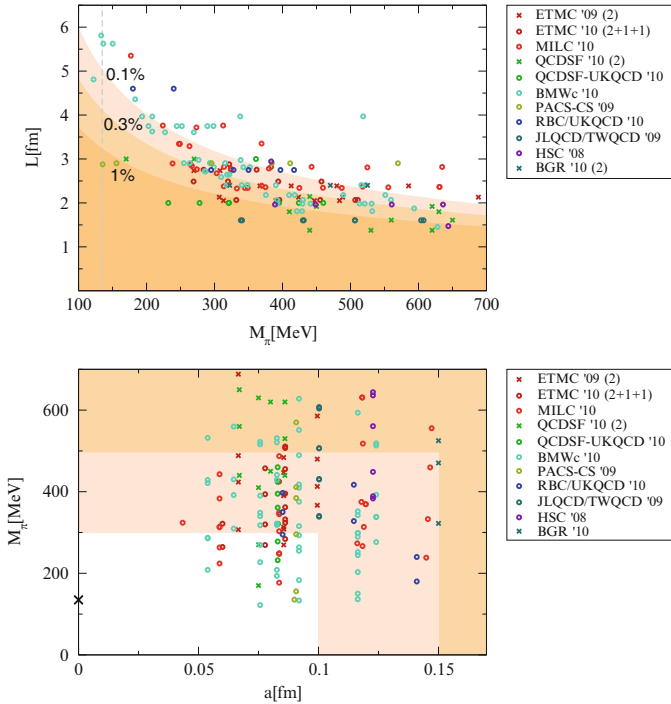


**Fig. 2.1** The landscape of recent dynamical lattice calculations, from Hoelbling’s review. The left plot shows the lattice extent  $L$  vs the pion mass. The physical pion mass is at the dashed line and the shading represents the relative error on the pion mass from 1 to 0.1 %. The right plot shows the pion mass,  $M_\pi$  vs the lattice spacing,  $a$ . The physical point is marked with a cross and the shading from dark to light indicates the more desirable parameter space for calculations

### 2.1.4 Correlators in a Euclidean Field Theory

Recall that in a Euclidean field theory, physical observables  $\mathcal{O}$  are evaluated as an expectation value over the relevant degrees of freedom

$$\langle \mathcal{O} \rangle = \frac{1}{Z} \left\{ \int \mathcal{D}U \mathcal{D}\Psi \mathcal{D}\bar{\Psi} \mathcal{O} e^{-S_{QCD}} \right\}. \quad (2.6)$$

The quark fields are Grassmann and are integrated out analytically, giving (with  $N_f = 2$ )

$$\langle \mathcal{O} \rangle = \frac{1}{Z} \left\{ \int \mathcal{D}U \det M^2 \mathcal{O} e^{-S_G} \right\}, \quad (2.7)$$

where  $S_G$  is the gauge action. The expectation value is then calculated by importance sampling of gauge fields and averaging over these ensembles. Typically, in hadron spectroscopy we are interested in two-point correlation functions built from interpolating operators, which are functions of the fields  $\Psi$ . A simple example is a local meson operator  $\mathcal{O}(x) = \bar{\Psi}_a(x) \Gamma \Psi_b(x)$ , where  $\Gamma$  is an element of the Dirac algebra with possible displacements and  $a, b$  are flavour indices.

The two-point function is then

$$C(\mathbf{x}, t) = \langle \mathcal{O}(x) \mathcal{O}^\dagger(0) \rangle = \langle \bar{\Psi}_a(x) \Gamma \Psi_b(x) \bar{\Psi}_b(0) \Gamma^\dagger \Psi_a(0) \rangle, \quad (2.8)$$

where I note that  $x \equiv (t, \mathbf{x}); t \geq 0$ .

Using Wick's theorem to contract the quark fields replaces the fields with propagators in the expression for the correlation function

$$\begin{aligned} C(\mathbf{x}, t) = & -\langle \text{Tr} (M_a^{-1}(0, x) \Gamma M_b^{-1}(x, 0) \Gamma^\dagger) \rangle \\ & + \delta_{ab} \langle \text{Tr} (\Gamma M_a^{-1}(x, x)) \text{Tr} (\Gamma^\dagger M_a^{-1}(0, 0)) \rangle. \end{aligned} \quad (2.9)$$

The trace is taken over spin and colour indices, which have been suppressed here for clarity.  $M_{(a,b)}^{-1}$  is the quark propagator.

Now, for flavour non-singlets (with  $a \neq b$ ) the second term above vanishes and the two-point correlation function can be written

$$C(\mathbf{x}, t) = \langle \text{Tr} (\gamma_5 M_a^{-1}(x, 0)^\dagger \gamma_5 \Gamma M_b^{-1}(x, 0) \Gamma^\dagger) \rangle. \quad (2.10)$$

To arrive at this expression we have also used  $\gamma_5$  hermiticity, namely that  $M^{-1}(x, y) = \gamma_5 M^{-1}(y, x)^\dagger \gamma_5$ , to rewrite the correlator in terms of propagators from the origin to all sites. These are the *point (to all) propagators* traditionally used in lattice calculations. In one final step we consider correlators in momentum space at zero momentum,

$$C(\mathbf{p}, t) = \sum_{\mathbf{x}} e^{i\mathbf{p}\cdot\mathbf{x}} C(\mathbf{x}, t) \quad (2.11)$$

$$\text{and } C(t) = C(\mathbf{p} = 0, t) = \sum_{\mathbf{x}} C(\mathbf{x}, t).$$

It is useful to bear in mind from what we have seen above that the fermion fields in the lagrangian are present in calculations of the fermion determinant and contribute to the integral over the gauge fields, while those fermion fields in measurements are manifest in calculations of the propagators. The integral over gauge fields is done using importance sampling and is not the subject of these lectures. We will however see more about techniques to determine the quark propagators.

For hadron spectroscopy the goal is to extract the energy of (colourless) states of QCD. This information is encoded in the two-point correlation functions which are discussed above and which I now write as

$$C(t) = \langle \phi_i(t) | \phi_j^\dagger(0) \rangle, \quad (2.12)$$

where,  $\phi_i$  and  $\phi_j^\dagger$  are operators acting on the quark fields to create a state at time  $t = 0$  and annihilate it at a later time  $t$ . Using the Euclidean time evolution of such operators,  $\phi(t) = e^{Ht} \phi e^{-Ht}$  and inserting a complete set of states allows us to write the correlator as

$$C(t) = \sum_{n=0}^{\infty} \frac{|\langle \phi | n \rangle|^2}{2m_n} e^{-E_n t}, \quad (2.13)$$

and note also that we are working in the low-temperature limit of QCD where  $\beta = 1/kT = L_t$  is large. From Eq. (2.13) it is easy to see that in the large time limit the exponential fall-off of the correlator gives the ground state energy,  $E_0$ , namely  $\lim_{t \rightarrow \infty} C(t) = Ze^{-E_0 t}$ . The usual procedure then is to fit correlators to an exponential and extract the ground state energy from the data at large times. A useful quantity in this respect is the effective mass, which can be defined as

$$a_t m_{\text{effective}} = -\log \left( \frac{C(t)}{C(t-1)} \right). \quad (2.14)$$

The effective mass should plateau at large time separations as the ground state exponential dominates in the correlator. This is illustrated in Fig. 2.2 which shows a single correlator and corresponding effective mass for the  $J/\Psi$  meson, determined on a  $12^3 \times 128$  anisotropic lattice. Note that for operators  $\phi_i = \phi_j$  in Eq. (2.12) the correlation function is positive definite and the effective mass converges monotonically from above.



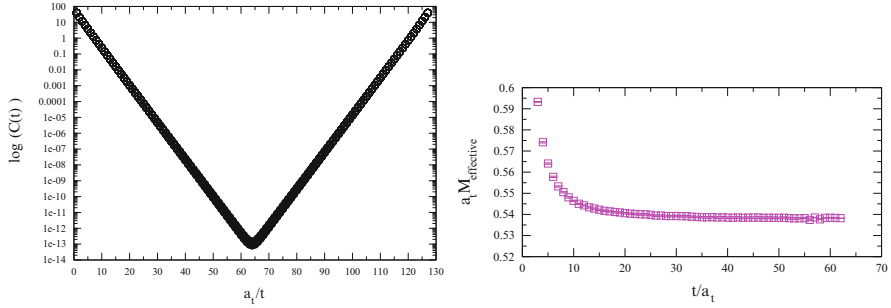


**Fig. 2.2** The left plot is a log plot of the correlator data, which is symmetric about the midpoint of the lattice for mesons under periodic boundary conditions. The right plot is the corresponding effective mass, determined using Eq. (2.14). Note that the data reach a plateau and remain constant from approximately timeslice twenty-five. At earlier times, excited state contamination in the form of additional exponentials is clearly visible

Now, it is clear from Eq. (2.13) that the correlation function contains information on all states that can be created by the operators used. However, the technique described above reliably gives the ground state while excited states, which would require more exponentials and more free parameters in a fit, very quickly become unreliable.

A different approach, designed to allow access to these excited states in a lattice calculation is the variational method, which I will return to in Sect. 2.4.2.3. The idea is that if we can measure a matrix of correlation functions

$$C_{ij}(t) = \langle 0 | \phi_i(t) \phi_j^\dagger(0) | 0 \rangle, \quad (2.15)$$

for all  $i, j$  and solve a generalised eigenvalue problem  $\mathbf{C}(t)\underline{v} = \lambda \mathbf{C}(t_0)\underline{v}$ , then the eigenvalues  $\lambda$  are related to the state energies by

$$\lim_{(t-t_0) \rightarrow \infty} \lambda_k = e^{-E_k t} + \mathcal{O}(e^{-\Delta E_n t}). \quad (2.16)$$

For this method to be practical we need (i) a good basis set of operators that resembles the states of interest and (ii) all elements of this correlation matrix measured [93]. In Sect. 2.4 we will look in more detail at the different approaches to operator construction which facilitate the variational approach.

## 2.2 Some New (and Old) Ideas for Making Measurements

To improve the precision and range of calculations that lattice methods can tackle let us take a closer look at quark propagators: the hadronic building blocks. In the previous section we saw that using time translational invariance and for flavour non-singlets a so-called point-to-all propagator can be calculated. The main advantage

of these propagators is that their calculation does not require vast computing resources. However, this comes at a hefty cost. Using point propagators restricts the accessible physics, making calculations of flavour singlets, where  $a = b$  in Eq. (2.9) (e.g. the  $\eta'$ ) and condensates impossible as these objects need propagators with sources everywhere in space. From a practical point of view point propagators restrict the interpolating basis used since a new inversion is needed for every operator that is not restricted to a single lattice point. Finally, from a philosophical point of view the point propagator entangles the propagator calculation and operator construction in a non-trivial way.

In this section I will discuss some different approaches used to calculate quark propagators: smeared point propagators, all-to-all propagators and distillation. Please see the references for a fuller description of these and other methods.

### 2.2.1 Smearing

Recall that hadrons are extended objects  $\mathcal{O}(1)$  fm whilst so far we have discussed the calculations of hadronic properties in terms of point-like propagators and interpolating fields. These may have small overlap with the state of interest, as determined by the amplitude  $\mathcal{Z}_n = \langle \phi | n \rangle$  appearing in Eq. (2.13). Improvements can be made by optimising the projection onto the state of interest using “smearing”: one uses an extended operator (for example of the form  $\bar{q}_x^{(1)} \Gamma \phi_{x,y} q_y^{(2)}$ ) where the function  $\phi_{x,y}$  is chosen to resemble a wavefunction. Essentially this works since the ground state wavefunction is smooth with no nodes.

This idea has been realised using Coulomb gauge fixing [94, 95] and by using iterative gauge-covariant smearing of the quark fields. This amounts to replacing

$$\Psi(x, t) = \sum_y \mathcal{G}(x, y, U(t)), \Psi(y, t), \quad (2.17)$$

where the function  $\mathcal{G}$  is the (Gaussian) smearing function given by  $\mathcal{G}(x, y, U(t)) = (1 + \kappa_s H)^{n_o}$  and  $H$  is frequently the lattice covariant Laplacian in three dimensions. Examples of iterative smearing procedures include Jacobi smearing [96] and Wuppertal smearing [97].

In addition, the gauge noise in a Monte-Carlo calculation can be significantly reduced by smearing the link, ( $U$ ) fields that appear in  $\mathcal{G}$ . Again, there are different approaches here including APE [98], HYP [99] and stout smearing [100].

Distillation [101], which will be more thoroughly discussed in Sect. 2.2.2.1 in the context of methods for all-to-all propagators can also be thought of as a variation or re-definition of smearing.

### 2.2.2 All to All Propagators

Let us turn now to consider methods for determining the quark propagator from all sites on the lattice to all sites. As already mentioned, point propagators restrict the accessible physics and we would like a robust method to go beyond this. To compute all elements of the quark propagator however would require full knowledge of the inverse and this is prohibitively expensive. Recall that the lattice representation of the Dirac operator is a large but sparse matrix and if we are satisfied with an unbiased estimator of all elements then sparse matrix methods can be used. Stochastic estimation should be acceptable—after all we are already using it to generate the gauge fields. We will also discuss later in this lecture the crucial role of variance reduction in these stochastic estimations.

To begin, we consider a spectral representation of the fermion matrix,  $Q = \gamma_5 M$ . This has the advantage that  $Q$  is hermitian and so its eigenvalues are easier to compute. If the eigenvalues and eigenvectors  $\{\lambda^{(i)}, v^{(i)}\}$  of  $Q$  can be computed then

$$Q = \sum_{i=1}^N \lambda^{(i)} v^{(i)} \otimes v^{*(i)} \quad \text{and so} \quad Q^{-1} = \sum_{i=1}^N \frac{1}{\lambda^{(i)}} v^{(i)} \otimes v^{*(i)}. \quad (2.18)$$

Unfortunately, finding even a small subset of eigenvectors is computationally expensive and so one is generally forced to truncate this representation for  $N_{ev} \ll N$ . This truncated sum now violates reflection positivity and must be corrected.

Let us go back and reconsider the fermion matrix,  $Q$ , by writing instead a stochastic representation of this matrix. This proceeds in the usual way: an ensemble of random independent noise vectors,  $\{\eta_{[1]}, \eta_{[2]}, \dots, \eta_{[N_r]}\}$  is generated with the property

$$\langle \langle \eta_{[r]}(x) \otimes \eta_{[r]}(y)^\dagger \rangle \rangle = \delta_{x,y}, \quad (2.19)$$

where the angle brackets indicate the expectation value over the distribution of noise vectors.  $Z_4$  is a good choice, noting that each component of the noise vectors has modulus 1, ie.  $\eta^{i\alpha}(x)^* \eta^{i\alpha}(x) = 1$  (with no summation), where  $i, j$  are colour indices and  $\alpha, \beta$  label spin.

The solution vectors,  $\Psi_{[r]}$  are obtained in the usual way

$$\Psi_{[r]}(x) = Q^{-1} \eta_{[r]}(y), \quad (2.20)$$

In this approach the quark propagator from any point  $x$  to any point  $y$  is written

$$Q^{-1}(y, x)_{\alpha\beta}^{ij} = \langle \langle \Psi_{[r]} \otimes \eta_{[r]}^\dagger \rangle \rangle_{\alpha\beta}^{ij} = \lim_{N_r \rightarrow \infty} \frac{1}{N_r} \sum_r^{N_r} \Psi_{[r]}^{i\alpha}(y) \eta_{[r]}^{j\beta}(x)^\dagger. \quad (2.21)$$

For  $N_r$  different sources the variance falls like  $1/\sqrt{N_r}$  and it would be useful to find methods that do better than this.

**Exercise** Verify that Eq.(2.21) indeed provides the inverse of the matrix  $Q$  by multiplying the equation on both sides with  $Q$ .

### 2.2.2.1 Variance Reduction by Dilution

In stochastic methods variance reduction is critical and it is useful to ask if the variance can be reduced below what has been mentioned. I will present one successful approach, called “dilution”.

Recall that the exact propagator can be computed with a finite (but large) amount of effort, namely by using point-propagators methods with Kronecker delta sources everywhere on the lattice. This suggests a trick. We break the vector space of the quark fields  $V$  into  $d$  smaller sub-spaces,  $V = V_1 \oplus V_2 \oplus \dots$  spanned by subsets of the basis vectors. This partitioning, called dilution, is arbitrary.

We can look at this in more detail. Dilute the noise vector  $\eta$  in some set of variables so that  $\eta = \sum_j \eta^{(j)}$ . For spectroscopy where temporal correlations are relevant an important example is time dilution which we can write as

$$\eta(\mathbf{x}, t) = \sum_{j=0}^{N_t-1} \eta^{(j)}(\mathbf{x}, t) \quad (2.22)$$

and  $\eta^{(j)}(\mathbf{x}, t) = 0$  unless  $t = j$ . Each diluted source is inverted, yielding  $N_d$  pairs of vectors  $\{\Psi^{(j)}, \eta^{(j)}\}$ . An estimator of  $Q^{-1}$  with a single noise source is then

$$\sum_{i=0}^{N_d-1} \Psi^{(i)}(\mathbf{x}, t) \otimes \eta^{(i)}(\mathbf{x}_0, t_0)^\dagger. \quad (2.23)$$

In the so-called “homeopathic limit” of dilution with a noise vector for each time, space, colour and spin component, the exact propagator is recovered in a finite number of steps. This of course is not practical in current simulations; however, the path through dilution space may be optimised so that the gauge field noise dominates for a manageable number of inversions.

It is also possible to incorporate dilution with the stochastic estimation in a hybrid method. Essentially the steps are: calculate  $N_{ev}$  eigenvalues and eigenvectors of  $Q$  exactly and determine  $Q_{N_{ev}}^{-1}$ ; use the stochastic method with dilution to correct the truncation. There are further details and a discussion of further optimisation in [102].

So, how does this dilution method compare with point propagators? The left pane of Fig. 2.3 shows the correlator for a light pseudoscalar determined on a  $12^3 \times 24$  lattice at  $\beta = 5.7$  with Wilson fermions and 75 gauge field configurations. The right pane shows an effective mass plot for three different states (the  $1^{+-}$ ,  $\rho$  and  $\pi$ )

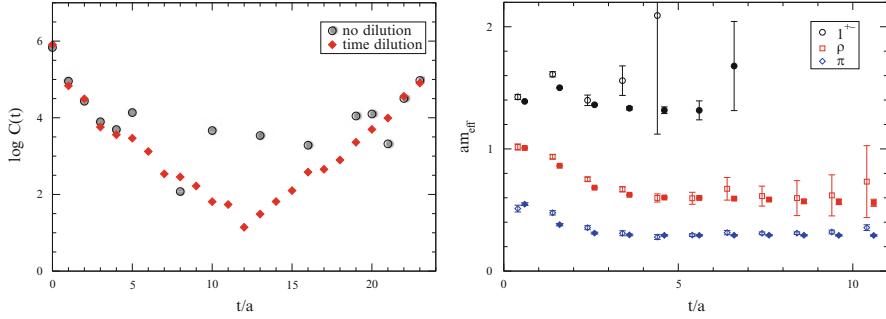


**Fig. 2.3** The left pane is a log plot of the correlator, as described in the text, comparing the point propagators with all-to-all propagators calculated using time dilution. The right pane shows the effective masses of three states again comparing the statistical precision of point and all-to-all propagators

determined on the same ensembles. Both plots are taken from [102]. The light quarks are relatively heavy with  $m_\pi/m_\rho = 0.50$ . One hundred eigenvectors were determined and dilution in time, space even-odd<sup>1</sup> and spin was implemented (in the right-hand plot). The plots show an impressive improvement in the statistical precision with which the correlator and effective masses are determined when using dilution (in time only) compared to traditional point sources.

### 2.2.3 Distillation

I will briefly describe a rather different approach to the determination of quark propagation, termed “distillation” [101]. Essentially the method is a redefinition of smearing (as described above) which as we will see leads to rather dramatic improvements in statistical precision and the range of accessible hadronic physics.

Consider a smeared quark field,  $\tilde{\Psi}$  derived from the “raw” quark field,  $\Psi$  in the path integral by  $\tilde{\Psi}(t) = \square[U(t)]\Psi(t)$ . The general expression for a (e.g. mesonic) creation operator is then

$$\mathcal{O}_M(t) = \bar{\tilde{\Psi}}(t)\Gamma\tilde{\Psi}(t), \quad (2.24)$$

where  $\Gamma$  is an operator in position, spin, colour space and the aim of smearing is to improve the overlap onto the state of interest.

<sup>1</sup>A cubic, or hypercubic, lattice may be divided into sublattices of “even” and “odd” sites, sometimes also referred to as checkerboarding. A lattice point,  $x \in \mathbb{Z}^4$  is even or odd depending on whether the sum of its coordinates  $x_\mu$  is even or odd. For details see for example the textbooks referenced.

Let us look in more detail at the smearing operator  $\square$ . Smearing is known to be very effective in building an operator that projects onto a low-lying hadronic state and a popular (gauge-covariant) algorithm is Gaussian smearing. A linear operator is applied,

$$\square_J = \exp(\sigma \nabla^2), \quad (2.25)$$

In this example  $\nabla^2$  is a lattice representation of the three-dimensional gauge-covariant laplace operator on the source time-slice.

$$\nabla_{x,y}^2 = 6\delta_{x,y} - \sum_{i=1}^3 U_i(x)\delta_{x+\hat{i},y} + U_j^\dagger(x-\hat{i})\delta_{x-\hat{i},y}. \quad (2.26)$$

Correlation functions built from such smeared operators then look like

$$\text{Tr} \square_J M^{-1} \square_J M^{-1} \square_J \dots \quad (2.27)$$

The key observation is that the Gaussian smearing operator acts as a projection operator on the space of coloured scalar fields on a time-slice ie  $N_S \times N_c$ . This is nicely seen by looking at the eigenvalues of the operator  $\nabla^2$  as shown in Fig. 2.4, taken from [101]. In brief then, distillation defines smearing to be explicitly a very low-rank operator, ie  $N_D \ll N_S \times N_c$ . The distillation operator is

$$\square(t) = V(t)V^\dagger(t), \quad (2.28)$$

and  $V_{\underline{x},c}^a(t)$  is an  $N_D \times (N_S \times N_c)$  matrix. One is free to choose a definition of  $\square$  and in studies to date it has been defined as  $\square_\Delta$  the projection operator into  $\mathcal{D}_\Delta$ , the space spanned by the lowest eigenmodes of the three-dimensional laplacian. This operator is idempotent so  $\square_\Delta^2 = \square_\Delta$  and it is also easy to see that  $\lim_{N_D \rightarrow (N_S \times N_c)} \square_\Delta = 1$ . Note however that this choice for  $\nabla^2$  is not unique. It does preserve lattice symmetries being translation, parity and charge-conjugation symmetric. It is  $O(3)$  symmetric and as discussed in [101] is close to  $SO(3)$  symmetric.

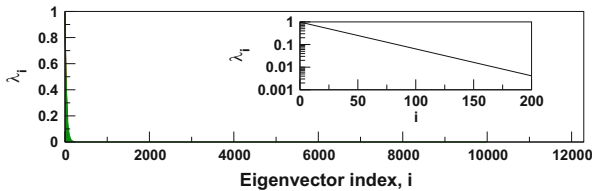


**Fig. 2.4** The eigenvalues of a Gaussian smearing operator. The main pane is the raw data, barely visible while the inset shows the first 200 modes on a log scale. Only the first  $\mathcal{O}(100)$  modes are significant. The data are determined on a  $16^3$  spatial volume

If we now consider an isovector meson two-point function

$$C_{\text{meson}}(t_1 - t_0) = \langle \langle \bar{u}(t_1) \square_{t_1} \Gamma_{t_1} \square_{t_1} d(t_1) \bar{d}(t_0) \square_{t_0} \Gamma_{t_0} \square_{t_0} u(t_0) \rangle \rangle, \quad (2.29)$$

then integrating over the quark fields yields

$$C_{\text{meson}}(t_1 - t_0) = \langle \text{Tr}_{\{\underline{x}, \sigma, c\}} (\square_{t_1} \Gamma_{t_1} \square_{t_1} M^{-1}(t_1, t_0) \square_{t_0} \Gamma_{t_0} \square_{t_0} M^{-1}(t_0, t_1)) \rangle. \quad (2.30)$$

Now, substituting the low-rank distillation operator for  $\square$  reduces this to a much smaller trace, written

$$C_{\text{meson}}(t_1 - t_0) = \langle \text{Tr}_{\sigma, \mathcal{D}} [\phi(t_1) \tau(t_1, t_0) \phi(t_0) \tau(t_0, t_1)] \rangle, \quad (2.31)$$

where both  $\phi_{\beta, b}^{\alpha, a}$  and  $\tau_{\beta, b}^{\alpha, a}$  are  $(N_\sigma \times N_{\mathcal{D}}) \times (N_\sigma \times N_{\mathcal{D}})$  matrices and

$$\phi(t) = V^\dagger(t) \Gamma_t V(t); \quad \tau(t, t') = V^\dagger M^{-1}(t, t') V(t'). \quad (2.32)$$

In the low-rank space, all elements of the reduced quark propagator are now accessible in a reasonable amount of compute time. As well as the reduction in compute time, distillation offers a second advantage: the separation of operator construction from quark propagation. Note that in Eq. (2.31) the function  $\tau(t, t')$ , known as the *perambulator*, contains the information on quark propagation while the  $\phi(t)$  describe the source and sink operators and determine the quantum numbers of the state to be constructed. The perambulators may be calculated and stored to be combined *a posteriori* with any number of source and sink operators. In addition, the number of eigenvalues used in  $\square$  may also be increased *a posteriori* without starting a calculation from scratch.

Distillation has proved particularly successful for calculations of isoscalar mesons, which traditionally have been difficult if not impossible to determine with precision. Figure 2.5 is taken from [103] and shows the disconnected contributions to the two-point correlation function, denoted  $\mathcal{D}$  for the  $\bar{\Psi} \gamma_5 \Psi$  operator in the light meson sector together with the connected contributions,  $\mathcal{C}$ . Figure 2.6 shows the corresponding isoscalar spectrum of light mesons.

While distillation offers a new avenue for precision spectroscopy it is not suitable for all hadronic physics. A particular example includes the strangeness content of the nucleon for which the standard all-to-all algorithms must be used.

In addition, the cost of distillation grows rapidly with the spatial volume of the lattice.  $N_{\mathcal{D}}$  scales with  $N_S$  and to maintain a constant resolution in the distillation space the cost of a calculation scales with  $V^2$ . Table 2.1 illustrates the cost scaling as a function of volume for mesons and baryons. However, the method has been successfully used on volumes up to  $24^3$  with  $N_{\mathcal{D}} = 128$  for a range of physics.

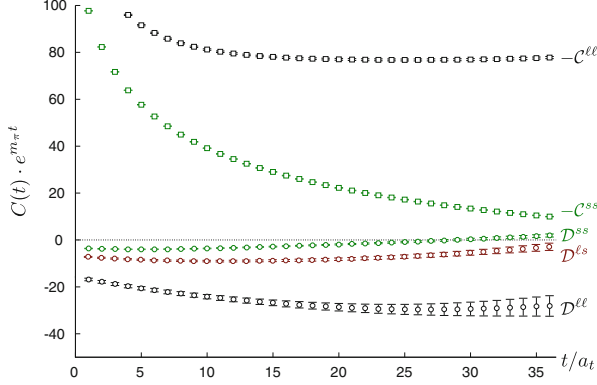


**Fig. 2.5** Distillation allows for precision calculation of disconnected contributions. The plot shows the connected as well as disconnected contributions, determined using distillation. Note the statistical precision and persistence of the signal for the disconnected diagrams

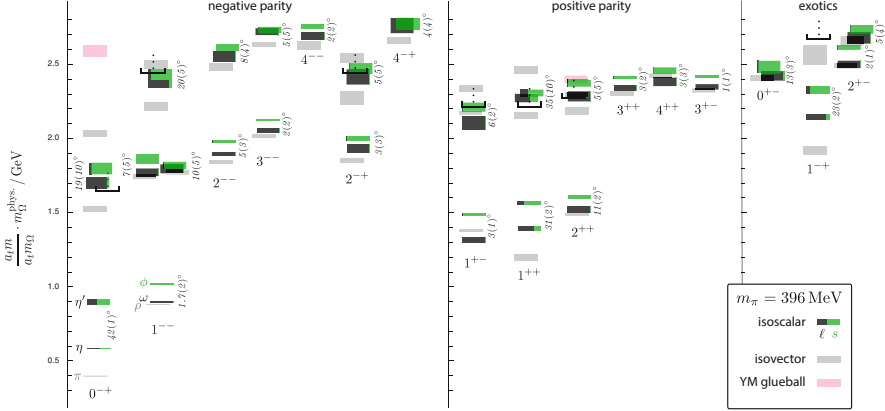


**Fig. 2.6** The light meson isoscalar spectrum from the Hadron Spectrum Collaboration

**Table 2.1** The cost scaling of distillation from inversions to contractions for mesons and baryons

Fermion solutions	Construct $\tau$	$\mathcal{O}(N_S^2)$
Operator constructions	Construct $\phi$	$\mathcal{O}(N_S^2)$
Meson contractions	$\text{Tr}[\phi \tau \phi \tau]$	$\mathcal{O}(N_S^3)$
Baryon contractions	$\bar{B} \tau \tau \tau B$	$\mathcal{O}(N_S^4)$

One solution, to mitigate the cost of distillation with increasing volume, is once again to use stochastic estimation techniques, together with distillation called stochastic LapH [104]. A stochastic identity matrix is constructed in the distillation space  $\mathcal{D}$  by introducing a vector  $\eta$  with  $N_{\mathcal{D}}$  elements and

$$E[\eta_i] = 0 \quad \text{and} \quad E[\eta_i \eta_j^*] = \delta_{ij}. \quad (2.33)$$



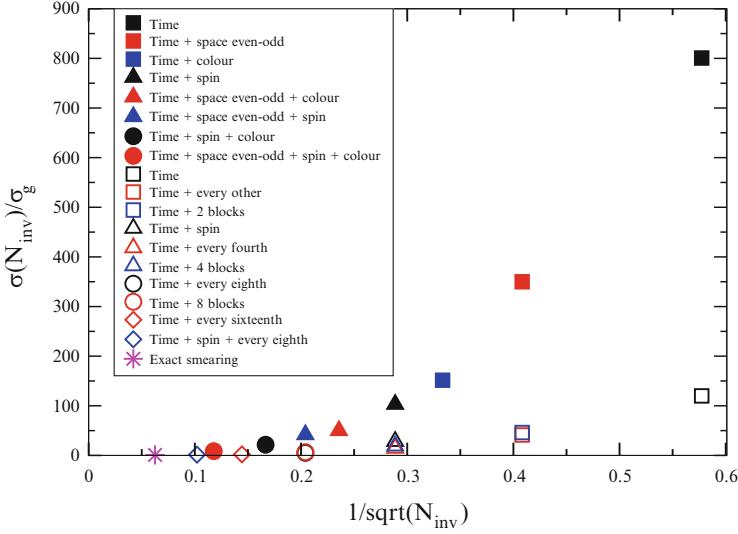


**Fig. 2.7** The ratio of the standard deviation from different stochastic estimators to the exact LapH estimate on time slice 5 for a nucleon correlator. Filled symbols denoted noise introduced on the entire lattice, open symbols use the “stochastic LapH” method outlined here

The distillation operator is then

$$\square = E[V\eta\eta^\dagger V^\dagger] = E[WW^\dagger]. \quad (2.34)$$

Of course this introduces noise into the computations and variance reduction once again becomes important. A good approach, as we saw earlier, is then to use dilution as before to “thin out” the stochastic noise. One can use  $N_{\mathcal{D}}$  orthogonal projectors to make a variance-reduced estimator of  $I_{\mathcal{D}} = E[WW^\dagger] = \sum_{k=1}^{N_{\mathcal{D}}} E[V\mathcal{P}_k\eta\eta^\dagger\mathcal{P}_k V^\dagger]$  with  $W_k = V\mathcal{P}_k\eta$  a  $N_{\mathcal{D}} \times (N_S \times N_C)$  matrix. Figure 2.7, taken from [105] demonstrates the improvements achieved using different dilution strategies for noise in distillation space for a baryon correlator compared to noise introduced across the entire lattice.

### 2.2.4 Interim Summary

In this section we have discussed methods to calculate quark propagation and make measurements. In this context it is useful to note that smearing and distillation are both rotationally symmetric operations and so do not change the quantum numbers of the states being determined. Algorithms which address the exponential fall in signal-to-noise in correlators and which reduce the cost of making measurements

are crucial. This is especially true for precision spectroscopy, the determination of exotic states and isoscalar mesons and for a strategy to include multi-hadron states in lattice calculations.

**Exercise** Do the linear algebra to derive Eqs. (2.30–2.31).

## 2.3 Lattice Symmetries and Classifying States

In continuum QCD observable states are classified according to angular momentum and parity,  $J^P$  which label the irreducible representations (irreps) of the relevant symmetry group: the improper rotation group  $O(3)$ . These irreps include bosonic (single-valued) and fermionic (double-valued) representations and in addition, the projection of angular momentum onto some axis,  $J_z$  labels rows of the representation.

On a spatially isotropic lattice the continuous rotational symmetry is broken and the relevant symmetry group is  $O_h$ , the cubic point group. Eigenstates of the lattice hamiltonian then transform under irreps of  $O_h$  and lattice states are classified by these irreps ( $\Lambda^P$ ) rather than by  $J^P$ . A manifestation of this symmetry breaking is that continuum states with the same  $J^P$  but different  $J_z$  values are in general separated across lattice irreps. It is important then to design operators which couple strongly to lattice eigenstates, i.e. which project into the irreps of  $O_h$ .

Now, let us consider the symmetry group of the cube in more detail. The correct group to consider is  $O$  the octahedral group which is dual to a cube. There are 24 rotational (orientation-preserving/proper) symmetries and 48 if one includes combinations of reflection and rotation. This leads us to consider the cubic point group  $O_h = O \otimes \{I, I_s\}$ .  $O$  has five conjugacy classes ( $O_h$  has 10) and the number of conjugacy classes gives the number of irreps. Using Schur's lemma for a group  $G$  and irreps  $\Gamma_i$  of  $G$ ,

$$|G| = \sum_i \dim(\Gamma_i)^2, \quad (2.35)$$

and a short calculation shows that for  $O$  we get:  $24 = 1^2 + 1^2 + 2^2 + 3^2 + 3^2$  the dimensions of the five irreps of  $O$  labelled  $A_1, A_2, E, T_1, T_2$  respectively. The extension to  $O_h$  includes the 24 improper rotations (spatial inversions) of  $O$  such that

$$I_s \begin{pmatrix} x \\ y \\ z \end{pmatrix} \rightarrow \begin{pmatrix} -x \\ -y \\ -z \end{pmatrix}. \quad (2.36)$$

The number of group elements is now 48 with 10 irreps labelled

$$A_{1g}, A_{1u}, A_{2g}, A_{2u}, E_g, E_u, T_{1g}, T_{1u}, T_{2g}, T_{2u}$$

and the  $(g, u)$  label the even (*gerade*) and odd (*ungerade*) behaviour under spatial inversion.

For baryons one considers  $O^D$ , the double cover of  $O$ . This 48-element group is obtained from  $O$  by including a negative identity (corresponding to rotations through  $2\pi$ ). Therefore  $O^D$  is the group through which the identity is recovered after rotation through  $4\pi$ . It has eight single-valued irreps, five of which correspond to irreps of  $O$ . The three new irreps are  $G_1, G_2, H$  and once again, using Schur's lemma we get  $24 = \sum_i \Gamma_i^2 = 2^2 + 2^2 + 4^2$  giving us the dimensions of the additional irreps (2, 2, 4 respectively).

Having briefly covered the properties of the relevant symmetry groups for mesons and baryons in lattice QCD the next section will discuss how a connection is made between the states identified in a lattice calculation and their continuum counterparts. I have not discussed group theory in detail and refer the reader to the many excellent textbooks some of which are listed here: [106–109].

### 2.3.1 Connecting Lattice and Continuum Groups

In this discussion, I will focus on  $O$  and meson states for simplicity, the procedure for the double cover group,  $O^D$  and baryons is the same.

In  $SO(3)$  there are an infinite number of irreps ( $J$  values) whereas for  $O$ , as we have just seen, there are just five irreps. Therefore there is not a one-to-one mapping between the irreps but rather lattice irreps may contain many states from different continuum irreps. To identify which continuum states can occur in a particular lattice irrep we note firstly that  $O$  is a subgroup of  $SO(3)$ . By restricting the irreps of  $SO(3)$  labelled by  $J$  to rotations allowed on a lattice we generate representations that are reducible ie  $J$  is reducible under  $O$  or  $O_h$ . This procedure is called subduction and using the relationship

$$n_J^{(\alpha)} = \frac{1}{N_G} \sum_k n_k \chi_k^{(\alpha)} \chi_k^{(J)}, \quad (2.37)$$

it is possible to find the multiplicity of the irreps of  $SO(3)$  in  $O$ . Note that in Eq.(2.37)  $\chi$  is the character of a representation,  $N_G$  is the order of the group and  $n_k$  is the dimension of the  $k$ th representation. Table 2.2 gives an example of this subduction process for continuum states up to  $J = 4$ . In principle then, to identify say a  $J = 2$  state, results from the  $E$  and  $T_2$  irreps at finite lattice spacing should be extrapolated to the continuum where for a particular state the results should agree. This is an expensive procedure, requiring simulations to be

**Table 2.2** The results of subduction showing the relationship between the continuum and lattice irreps, up to  $J = 4$ . Note that as discussed in the text a continuum spin may appear in a number of lattice irreps making spin identification for states with  $J > 1$  complicated

	$A_1$	$A_2$	$E$	$T_1$	$T_2$
$J = 0$	1				
$J = 1$				1	
$J = 2$			1		1
$J = 3$		1		1	1
$J = 4$	1		1	1	1
$\vdots$	$\vdots$	$\vdots$	$\vdots$	$\vdots$	$\vdots$

repeated at multiple lattice spacings. Even if this were feasible it is not guaranteed to yield an unambiguously determined state. Consider the following example in the charmonium system. From Table 2.2 we see that a spin four state,  $4^{++}$  should appear, at finite  $a$ , in the  $A_1, E, T_1, T_2$  irreps. However, in charmonium there is also a near-degenerate triplet of  $P$  waves with quantum numbers  $(0^{++}, 1^{++}, 2^{++})$  which are distributed across the same irrep pattern, namely  $A_1, E, T_1, T_2$ . In a lattice calculation, even after extrapolation to the continuum limit, it would be extremely difficult, if not impossible, to disentangle a radial excitation of this triplet from the  $4^{++}$  ground state without some additional information. Before I discuss how to tackle this problem let me briefly mention the group theory of two particles in a box. This, of course, is relevant once states above threshold are considered where multi-hadron operators must be included. In general, for mesons in flight the relevant symmetry group is reduced to the little group of allowed cubic rotations that leave the momentum invariant. There is a detailed description in [110, 111].

## 2.4 Building Operators and Extracting Energies

In this chapter we have spent some time looking at different methods for quark propagation. Now, we will discuss operator construction and how to extract energies from the correlation functions determined in a lattice calculation. The meson and baryon operators are generally of the form  $\mathcal{O} = \bar{\Psi}_{i\alpha}(\mathbf{x}, t) \Gamma_{\alpha\beta} \Psi_{i\beta}(\mathbf{x}, t)$  and  $\mathcal{O} = \epsilon^{abc}(\Psi^a(\mathbf{x}, t) \Gamma \Psi^b(\mathbf{x}, t)) \Psi^c(\mathbf{x}, t)$ .

The simplest operators we can consider are colour-singlet local fermion bilinears such as  $\mathcal{O}_\pi = \bar{d} \gamma_5 u$  and  $\mathcal{O}_\rho = \bar{d} \gamma_i u$  for mesons and  $\mathcal{O}_N = \epsilon^{abc}(u^a C \gamma_5 d^b) u^c$  and  $\mathcal{O}_\Delta = \epsilon^{abc}(u^a C \gamma_\nu d^b) u^c$  for baryons. The local operators written here give access to states with  $J = 0, 1, \frac{1}{2}, \frac{3}{2}$ . While one can choose different Dirac structures  $\Gamma$  the spin and parity of the hadrons will put constraints on the number of operators that

can be constructed. To study higher-spin states with  $J > 1$  (mesons) and  $J > 3/2$  (baryons) additional operators must be used. In addition we would like many more operators that all transform irreducibly under some irrep, enabling a variational analysis.

One approach, using smearing techniques described in Sect. 2.2.1 is to use smearing functions of different widths. Combining these sources can generate nodes in the wavefunctions to better overlap with (radially) excited states. See for example [112] for a discussion and results.

Another approach (and one which can be combined with different smearings) is to use extended operators. Recall that lattice operators are bilinears, with path-ordered products between the quark (and the anti-quark) fields. Different offsets, connecting paths and spin contractions give different projections into lattice irreps. Further simple examples are given in Fig. 2.8 for mesons and in Fig. 2.9, taken from [113], for baryons. In this way one can make arbitrarily complicated operators to access high-spin states and to allow for a variational analysis. An early success of this approach was a determination of the Yang-Mills glueball spectrum [77]. QCD is a non-abelian gauge theory and so allows bound states of pure glue. In this case the interpolating fields are purely gluonic and built from Wilson loops, as shown in Fig. 2.10. The spectrum which was extracted using these operators is also shown in Fig. 2.10. Note that states with spin up to  $J = 3$  were determined.

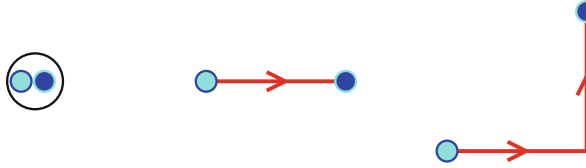


**Fig. 2.8** Meson operators. Written in full these are  $\mathcal{O}_{\alpha\beta} = \sum_x \bar{\psi}_\alpha(x) \psi_\beta(x)$ ,  $\mathcal{O}_{\alpha\beta}^i = \sum_x \bar{\psi}_\alpha(x) U_i(x) \psi_\beta(x + \hat{i})$ ,  $\mathcal{O}_{\alpha\beta}^{ij} = \sum_x \bar{\psi}_\alpha(x) U_i(x) U_j(x + \hat{i}) \psi_\beta(x + \hat{i} + \hat{j})$  respectively

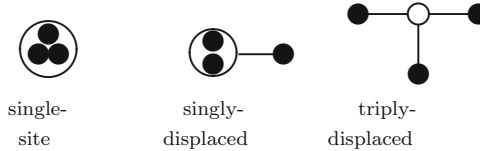


**Fig. 2.9** Three different prototype extended baryon operators. The *hollow circle* is the reference site

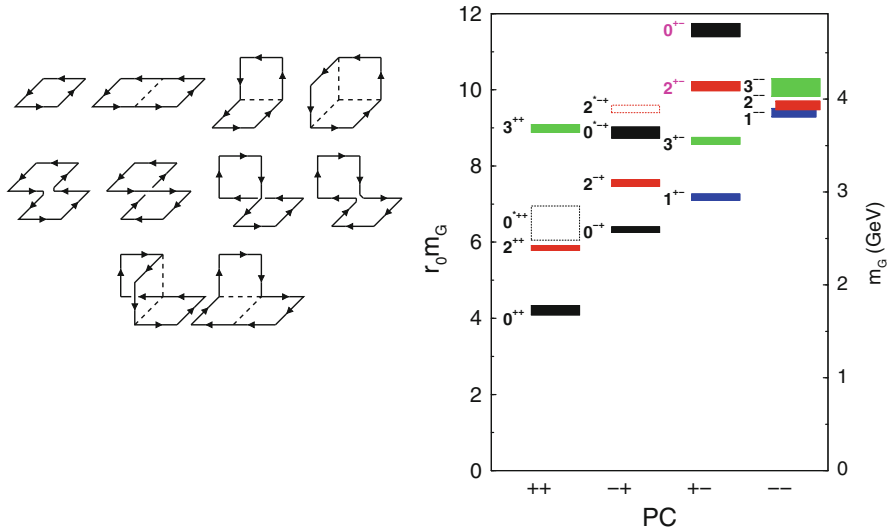


**Fig. 2.10** A selection of operators for glueball spectroscopy. These were used in a variational calculation to determine the (quenched) glueball spectrum shown in the right plot

### 2.4.1 Constructing Good Operators

We have seen how operators of arbitrary complexity can be calculated to access, in principle, high-spin states. However, it is useful to ask what makes a “good” operator in order to maximise the statistical precision and to ensure reliable state identification at finite lattice spacing. A useful list of properties for operators includes

1. have definite momentum and transform under the symmetries of a lattice irrep
2. the basis of operators used should have a good overlap with the states of interest (eigenvectors of the variational method) which are, or are close to being, linearly independent
3. not noisy ie produce a correlator with acceptable statistical precision over a reasonable number of timeslices

On the last point we have seen how to improve statistical precision using smearing and distillation as well as noise reduction in all-to-all propagators using e.g. dilution.

Now, recall that in an earlier lecture we discussed the relationship between lattice and continuum irreps. If we now rewrite Table 2.2 we see that a correlator,  $C(t) = \langle 0 | \phi(t) \phi^\dagger(0) | 0 \rangle$ , contains in principle information about all (continuum) spin states that appear in a lattice irrep,  $\Lambda^{PC}$  (Table 2.3).

The objective is to build a basis of good operators according to the bullet points listed earlier in this section. There are different approaches to optimising lattice operators and I present one here [114].

**Table 2.3** The relationship between lattice and continuum irreps, determined by subduction. The table illustrates that lattice operators that transform according to a lattice irrep will contain information about more than one continuum spin state

Lattice irrep, $\Lambda$	Dimension	Continuum irreps, $J$
$A_1$	1	0, 4, ...
$A_2$	1	3, 5, ...
$E$	2	2, 4, ...
$T_1$	3	1, 3, ...
$T_2$	4	2, 3, ...
$G_1$	3	$\frac{1}{2}, \frac{7}{2}, \dots$
$G_2$	3	$\frac{5}{2}, \frac{7}{2}, \dots$
$H$	4	$\frac{3}{2}, \frac{5}{2}, \dots$

We begin by considering continuum operators built from  $n$  derivatives of the form

$$\phi = \bar{\Psi} \Gamma (D_{i1} D_{i2} D_{i3} \dots D_{in}) \Psi. \quad (2.38)$$

Construct irreps of  $SO(3)$  and then subduce these representations into  $O_h$ . Now replace the derivatives with lattice finite differences such that

$$D_j \Psi(x) \rightarrow \frac{1}{a} \left( U_j(x) \Psi(x + \hat{j} - U_j^\dagger(x - \hat{j}) \Psi(x - \hat{j}) \right), \quad (2.39)$$

where we note that on a discrete lattice, covariant derivatives become finite displacements of quark fields connected by links.

The final step is the empirical observation, with for example a more detailed discussion in [115], that the overlaps  $\mathcal{Z} = \langle 0 | \phi^{A^{PC}} | J^{PC(\Lambda)} \rangle$  in the different lattice irreps subduced from a common continuum irrep are the same up to rotation-breaking effects.

To see this explicitly let us consider an operator for the  $J^{PC} = 2^{++}$  meson. Recall from Table 2.2 that a spin two state will be split across the  $T_2$  and  $E$  lattice irreps. In the continuum an operator that creates a state with  $2^{++}$  quantum numbers is

$$\phi_{ij} = \bar{\Psi} \left( \gamma_i D_j + \gamma_j D_i - \frac{2}{3} \delta_{ij} \gamma \cdot D \right) \Psi. \quad (2.40)$$

Following the recipe described above we substitute gauge-covariant lattice finite differences for  $D$ . By subduction we find that

$$\begin{aligned} \phi^{T_2} &= \{\phi_{12}, \phi_{23}, \phi_{31}\}, \\ \phi^E &= \left\{ \frac{1}{\sqrt{2}}(\phi_{11} - \phi_{22}), \frac{1}{\sqrt{6}}(\phi_{11} + \phi_{22} + \phi_{33}) \right\}. \end{aligned}$$

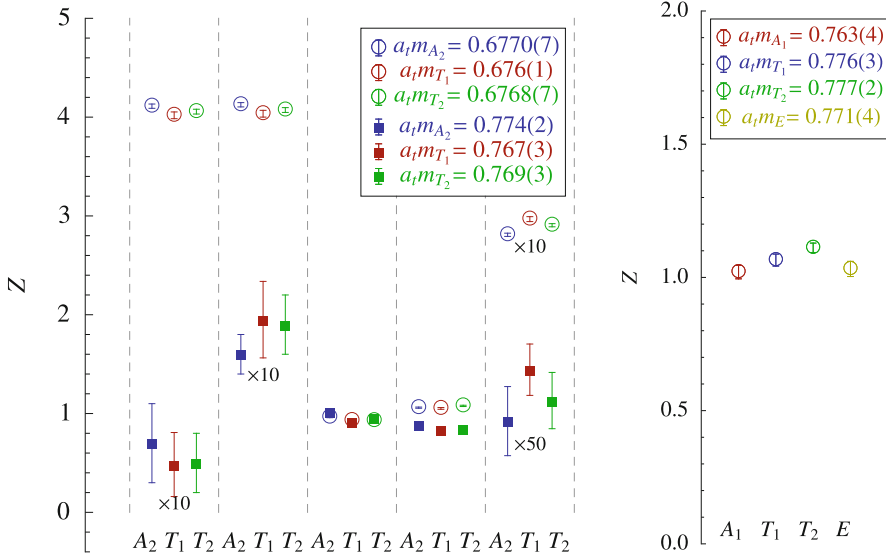


**Fig. 2.11** An example of the agreement of overlaps of lattice operators from different irreps which have been subduced from the same continuum operator. For more details see [116] and references therein

States determined from variational analyses in these two different irreps should then agree in the continuum limit and at finite  $a$  be reasonably close, assuming (hopefully) small discretisation effects. A second tool at finite  $a$  is to examine the operator overlaps  $Z$  for the signature of continuum symmetry

$$Z = \langle 0 | \phi^{(T_2)} | 2^{++(T_2)} \rangle = \langle 0 | \phi^{(E)} | 2^{++(E)} \rangle, \quad (2.41)$$

up to rotation-breaking effects. This approach has been followed by the Hadron Spectrum Collaboration to good effect. Figure 2.11 taken from [116] shows this operator overlap analysis for spin three and spin four states in charmonium. In each case there is very good agreement across the relevant irreps ( $A_2, T_1, T_2$  for  $J = 3$  and  $A_1, T_1, T_2, E$  for  $J = 4$ ).

#### 2.4.2 Fitting Data to Extract Energies

Hadron energies are determined from 2-point correlation functions. We begin by considering a simple correlator of the form

$$C(\mathbf{p}, t) = \sum_{\mathbf{x}} e^{i \mathbf{p} \cdot \mathbf{x}} \langle \mathcal{O}(\mathbf{x}, t) \mathcal{O}^\dagger(\mathbf{0}, t) \rangle, \quad (2.42)$$



where  $\mathcal{O}$  is a single interpolating operator for the hadron of interest. Recall that by inserting a complete set of energy eigenstates  $|n\rangle$  and assuming a discrete energy spectrum as  $t \rightarrow \infty$  and for hadrons at rest

$$C(t) \rightarrow \frac{1}{2E_n} |\langle 0 | \mathcal{O} | n_0 \rangle|^2 e^{-E_0 t}, \quad (2.43)$$

where  $n_0$  is the lightest state that couples to  $\mathcal{O}$  and has energy  $E_0$ .

Again, recall that a useful quantity for this analysis is the *effective mass*

$$a_t M_{\text{eff}}(t) = \ln \left( \frac{C(t)}{C(t+1)} \right) \xrightarrow{t \rightarrow \infty} \text{constant}, \quad (2.44)$$

and an alternative definition appropriate for mesons, under periodic boundary conditions, uses the hyperbolic cosine and is given by

$$a_t M_{\text{eff}}(t) = \cosh^{-1} \left( \frac{C(t+1) + C(t-1)}{2C(t)} \right). \quad (2.45)$$

At large time separations on the lattice the ground state dominates and the effective mass should plateau at this energy. Of course the onset and length of the plateau will depend on  $\mathcal{O}$ . The hadron mass is extracted from fits to correlator data in this plateau region. Such fits require some finesse however since statistical errors grow exponentially with  $t$  (except in the case of the pion) and fitting too far out in the temporal extent increases the statistical uncertainty.

Figure 2.12 shows a typical effective mass plot—in this case for the vector  $J/\Psi$  charmonium state. The cyan box highlights the plateau region, at large times, where the effective mass converges to the ground state. In this region the correlator data is fitted to the expected form,  $C(t) = Ae^{-E_0 t}$  using, for example, a  $\chi^2$  minimisation algorithm with  $A$  and  $E_0$  free parameters and for some “reasonable” choice of time

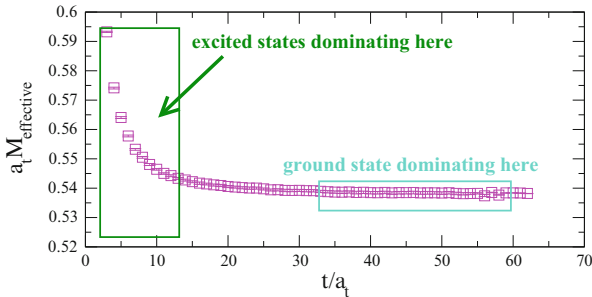


**Fig. 2.12** The same plot as in Fig. 2.2 now with the plateau region and the region of excited state contamination highlighted

range. Statistical errors on the fitted energy can be determined using bootstrap or jackknife (described later). The plot also shows a region where excited state energies are significant and a single-exponential fit would not be reasonable.

### 2.4.2.1 Resampling Techniques

Bootstrap and Jackknife are examples of what is known as resampling and both are used extensively to estimate statistical errors in lattice calculations.

The jackknife method was introduced by Quenouille in 1949 to estimate the bias of an estimator and later further refined by Tukey (who also gave us the FFT) in 1957. Consider a set of  $N$  measurements, and remove the first leaving a jackknifed set of  $N - 1$  resampled measurements. Repeat the analysis (in our case the exponential fits) on this reduced set, giving parameters  $\alpha_{J(1)}$ . The resampling is repeated, discarding the second measurement etc to get a set of parameters  $\alpha_{J(i)}$ ,  $i = 1, \dots, N$ . The statistical error is then estimated from averages over the resampled set

$$\sigma_J^2 = \frac{(N-1)}{N} \sum_{i=1}^N (\alpha_{J(i)} - \alpha)^2, \quad (2.46)$$

where  $\alpha$  is the result from fitting the full dataset.

The second resampling technique is the bootstrap method, developed by Efron in the late 1970s. In this case a new dataset is created by drawing  $N$  datapoints, with replacement, from the original dataset of size  $N$ . Replacement means that a configuration may appear twice in a sample; thus you do not get the original set each time but a set with a random fraction of the original points with some appearing multiple times. As for the jackknife method, the analysis is repeated on each set.

### 2.4.2.2 Notes on Fitting

When fitting correlator data to exponentials a good fit can be characterised by a few measures

1. the fit should be stable with respect to the choice of time range in the plateau region. In particular, it should be stable with respect to small changes in  $t_{\min}$ , the minimum timeslice included in the fit.
2. the fit should include a reasonable range in  $t$ . The number of points included will of course depend on the temporal extent and resolution of the lattice.
3. the energy extracted should be stable if additional exponentials are added to the fitting function.
4. for correlated fits, a good  $\chi^2/N_{\text{d.o.f.}}$ , typically of order one when this quantity can be reliably determined.
5. “reasonable” statistical errors on the fitted mass.

Within the lattice QCD community there are some well-established quantities which are used to describe the quality of fits, including

1. a sliding window plot: the fitted mass is plotted as a function of  $t_{\min}$ . A plateau region in this plot means the fitted mass is stable as a function of  $t_{\min}$ .
2. a fit histogram: the idea is to design a quantity that monitors the behaviour of a good fit as described above. An example is to plot  $QN_{\text{d.o.f.}}/(\Delta m)$  for each  $(t_{\min}, t_{\max})$  with  $Q = \Gamma[(\text{interval} - N_{\text{param}})/2, \chi^2/2]$  and choose the  $(t_{\min}, t_{\max})$  that maximises this quantity.
3.  $\chi$ -by-eye: always a good idea to check fit ranges do look reasonable on the effective mass plots.

The analysis discussed so far is focused on determinations of ground state energies. Looking again at the sample effective mass plot, shown in Fig. 2.12, it is clear that while a single exponential dominates at large times, at short time separations there are contributions from higher excited states in the form of additional exponentials in the correlation function

$$C(t) = Ae^{-E_0 t} + Be^{-E_1 t} + \dots \quad (2.47)$$

A two-exponential fit with parameters  $A, B, E_0, E_1$  may allow for a determination of  $E_1$ , the energy of the first excited state. A reasonable approach since the regions where  $E_0$  and  $E_1$  are distinct is to fit for  $E_0$  as described, and freeze its value in a fit for  $E_1$ . However, these two exponential fits can be very unstable and a different approach is needed especially to extract energies above just the first excited state. There are a number of techniques for this including Bayesian analysis;  $\chi^2$ -histogram analysis and a variational analysis. I will discuss the latter in more detail.

### 2.4.2.3 A Little More on Variational Analysis

We have already seen the basics of a variational analysis and is described in [117, 118] and [93]. In a brief recap we consider a basis of operators  $\mathcal{O}_i$  for  $i = 1, \dots, N$  in a given lattice irrep. Form a matrix of correlators

$$C_{ij}(t) = \langle \mathcal{O}_i(t) \mathcal{O}_j^\dagger(0) \rangle, \quad (2.48)$$

and treat this system as a generalised eigenvalue problem

$$C(t)\mathbf{v}_n(t, t_0) = \lambda_n(t, t_0)C(t_0)\mathbf{v}_n(t, t_0), \quad (2.49)$$

where  $t_0$  is a reference timeslice which you choose. The vectors  $\mathbf{v}_n$  diagonalise  $C(t)$  and for finite  $N$  one can show that a generalised effective mass is

$$E_n^{\text{eff}}(t, t_0) = -\partial_t \log \lambda_n(t, t_0) = E_n + O(e^{-\Delta E_n t}). \quad (2.50)$$

The eigenvalues  $\lambda_n$  that are solved for in the GEVP and ordered such that  $\lambda_1(t) > \lambda_2(t) > \dots \lambda_N(t)$  at large  $t$ . The  $\lambda_i$  are then related to the energies of the states in the irrep and these energies can be extracted from fits to the “principal correlators”. When using jackknife or bootstrap techniques the eigenvectors resulting from the GEVP should also be monitored to maintain a consistent ordering in the samples. Note that the procedure depends on the choice of reference timeslice,  $t_0$ . In an analysis this parameter should be varied to test the robustness of results. In particular, if the value of  $t_0$  is too small then states with energies larger than that of interest, say  $E_n$  will contaminate the results. This is especially true if there is just a small energy gap to  $E_{n+1}$  and in this case a large distance in  $t$  will be needed to resolve a plateau. Values of  $t_0$  too large may result in numerical instabilities.

#### 2.4.2.4 Anisotropic Lattices

Let me make a brief comment here on the utility of anisotropic lattices for hadron spectroscopy. If we can build a good basis of operators we have seen how we can extract energies for low-lying states from the correlator at short distances. The lattice correlator can only be sampled at discrete values of  $t$  and signal can fall quickly for a massive state, while the statistical noise does not. A brute force approach to reduce the lattice spacing in all directions is a costly solution to this problem. Nevertheless one can mitigate the cost by reducing the temporal lattice spacing,  $a_t$  whilst keeping the spatial mesh coarse. This is an anisotropic lattice.

Of course, the anisotropic lattice reduces the symmetries of the theory from the hypercubic to the cubic point group and for example, the dimension four operators on the lattice are split

$$\begin{aligned} \text{Tr} F_{\mu\nu} F_{\mu\nu} &\rightarrow \{\text{Tr} F_{ij} F_{ij}, \text{Tr} F_{i0} F_{i0}\} \\ \bar{\Psi} \gamma_\mu D_\mu \Psi &\rightarrow \{\bar{\Psi} \gamma_i D_i \Psi, \bar{\Psi} \gamma_0 D_0 \Psi\}. \end{aligned}$$

Note that on the  $3 \oplus 1$  anisotropic lattice described here the spatial symmetries are unchanged from the isotropic case and the group theory and operator construction discussions from earlier sections are unchanged.

There is a cost to this approach however. The space-time symmetry breaking introduces extra bare parameters in the lagrangian, arising from the so-called aspect ratio,  $\xi = a_s/a_t$ , which must be tuned to restore Euclidean rotational invariance in the continuum limit. For QCD one can think of this as demanding that quarks and gluons “feel” the same anisotropy. This requires an *a priori* tuning of parameters. In dynamical QCD where the fermions contribute through the determinant term in the path integral two physical conditions, one in the gauge sector and one in the fermion sector, must be simultaneously satisfied. A typical example uses the sideways potential and the pion dispersion relation. Each time the lattice spacing (temporal or

spatial) is changed the tuning must be repeated. In addition taking a continuum limit is challenging as one should consider the temporal and spatial spacings separately. Nevertheless, the anisotropic lattice as proved extremely effective for resolving precisely the energy levels of hadrons from light to heavy.

### 2.4.3 *A Lattice Error Budget*

In this section I have not discussed the standard systematic uncertainties which must be accounted for in a lattice calculation. These effect all lattice calculations, not specifically hadronic quantities and have also been discussed elsewhere at this School. They include lattice artefacts: which require an extrapolation to the continuum limit,  $a \rightarrow 0$ ; finite volume effects: in spectroscopy energy measurements can be distorted by the finite box. A rule of thumb is that  $m_\pi L > 3$  is reasonable for many quantities; unphysically heavy pions: simulations at the physical point are now a reality but most calculations still rely on chiral extrapolation to reach physical up and down quark masses. Chiral perturbation theory (ChPT) is used to guide these extrapolations but an open question is whether chiral corrections are reliably described by ChPT; Fitting uncertainties: the choice of fit range and  $t_0$  and how to choose these quantities has been discussed above.

## 2.5 Current Challenges

In this final section I would like to discuss some challenges for lattice hadron spectroscopy. I will focus on one topic: resonances and scattering. The most recent progress on this (and other topics in spectroscopy) has been described in plenary and parallel sessions at Lattice 2013 [119].

### 2.5.1 *Resonances and Scattering States*

In this chapter we have assumed that all particles in the spectrum are stable, and that quark bilinears or three-quark operators are a reliable way to reproduce the states of interest. However, the majority of states are not stable and are in fact resonances or scattering states. A resonance is a state that forms for example when colliding two particles and which then decays quickly to scattering states. Resonances respect conservation laws: if the isospin of the colliding particles is  $\frac{3}{2}$  then the resonance must have isospin  $\frac{3}{2}$  (a  $\Delta$  resonance). They are usually indicated by a sharp peak in a cross-section as a function of the centre-of-mass energy of the collision.

A challenge for lattice QCD is to distinguish and describe resonances and scattering states. The difficulty for lattice calculations lies in the Maiani-Testa no-go theorem [120]. Recall that importance sampling in Monte-Carlo simulations relies on having a path integral with positive definite probability measure, which is the motivation for the Wick rotation to Euclidean space. However, the Maiani-Testa theorem states that in general, scattering matrix ( $S$ -matrix) elements cannot be extracted from infinite-volume Euclidean-space correlation functions. In Minkowski space the  $S$ -matrix elements are complex functions, above kinematic thresholds. However, in a Monte-Carlo calculation (in Euclidean space) these matrix elements are real and there is no distinction between the  $|in\rangle$  and  $|out\rangle$  states and information about the phase due to final-state interactions is lost. Lüscher showed how information about elastic scattering can be inferred from the volume-dependence of the spectrum. The formalism for the relativistic (elastic) case in a cubic box for a system at rest is described in [117, 121] and was subsequently extended to moving frames in [122–124].

This has led to renewed progress in recent years in studies of scattering states and resonances which has been enabled by some of the new techniques described in these lectures. In particular, to be able to determine volume-dependence reliably it is crucial to have precise data and unambiguous spin-identification so that two-hadron states can be distinguished from nearby excited states.

### 2.5.1.1 The Lüscher Formalism

In general, on a finite lattice with periodic boundary conditions the hadron momenta are quantised:  $\underline{p} = \frac{2\pi}{L} \{n_x, n_y, n_z\}$ , with  $n_i \in \{0, 1, 2, \dots, L-1\}$ , and the energy spectrum is a set of discrete levels, classified by  $\underline{p}$ . The allowed energies, for a particle of mass  $m$  are

$$E = \sqrt{m^2 + \left(\frac{2\pi}{L}\right)^2 N^2}, \quad \text{where } N^2 = n_x^2 + n_y^2 + n_z^2. \quad (2.51)$$

The density of states in such systems will increase with energy since there are more momenta combinations for a given  $N^2$  e.g. both  $(3, 0, 0)$  and  $(2, 2, 1)$  correspond to  $N^2 = 9$ . It is also of course possible to construct a system with zero total angular momentum from two hadrons with back-to-back momentum,  $\underline{p}$  and  $-\underline{p}$ .

A brief example is given by the  $\rho \rightarrow \pi\pi$  system. The energy levels of two non-interacting pions in a periodic box of length  $L$  are

$$E = 2\sqrt{m_\pi^2 + p^2}, \quad p = \frac{2\pi|\mathbf{n}|}{L} \quad (2.52)$$

where as usual  $\mathbf{n}$  has components  $n_i \in \mathbb{Z}$ . Considering the interacting case, the energy levels are

$$E = 2\sqrt{m_\pi^2 + p^2}, \quad p = \left(\frac{2\pi}{L}\right)q \quad (2.53)$$

where  $q$  is no longer constrained to originate from a quantised momentum mode. Therefore the energy eigenvalues will deviate from the noninteracting case. These deviations contain information about the underlying strong interaction and yield resonance information via the Lüscher formalism described by

$$\delta(p) = -\phi(q) + \pi n, \quad (2.54)$$

where

$$\tan \phi(q) = -\frac{\pi^{3/2}q}{Z_{00}(1;q^2)} \quad \text{and} \quad q = \frac{pL}{2\pi}. \quad (2.55)$$

As usual,  $p_n$  is defined for level  $n$  with energy  $E_n$  from the dispersion relation  $E_n = 2\sqrt{m^2 + p_n^2}$ . The  $Z_{00}$  is a generalised Zeta function given by [125]

$$Z_{jm}(s, q^2) = \sum_{n \in \mathbb{Z}^3} \frac{r^j Y_{jm}(\theta, \phi)}{(n^2 - q^2)^s}. \quad (2.56)$$

Once the phase shift is determined and for a well-defined resonance, one can fit a Breit-Wigner to extract the resonance width  $\Gamma_\rho$  and mass  $m_\rho$ ,

$$\frac{p^3}{E} \cot \delta(p) = -\frac{p_\rho^3}{m_\rho^2 \Gamma_\rho} (E^2 - m_\rho^2), \quad p_\rho = \frac{1}{2} \sqrt{m_\rho^2 - 4m_\pi^2}. \quad (2.57)$$

To extract these energy shifts one needs good operators for both single-hadron and multi-hadron states. Distillation has proved a crucial tool in this regard. Our example,  $\rho \rightarrow \pi\pi$ , is in isospin one, and in principle this involves disconnected diagrams which, as already discussed, add additional complexity to lattice calculations. One can learn a lot however, by looking at the simpler  $I = 2$ ,  $\pi\pi$  system. The Hadron Spectrum Collaboration has produced a detailed study of this system including many operators to map out the phase shift in great detail. Figure 2.13 shows the energy shifts in  $I = 2$   $\pi\pi$  scattering from [126]. The phase shift (for  $l = 0$ , the lowest wave and  $l = 2$ ) has been calculated for many different momenta and different volumes as shown in Fig. 2.14. More recently [127], the  $I = 1$  phase shift has been mapped out in great detail and a resonance width and mass extracted. There are already similar calculations in the open charm sector both with much fewer momenta points or lower statistics [128, 129]. More can be expected in the

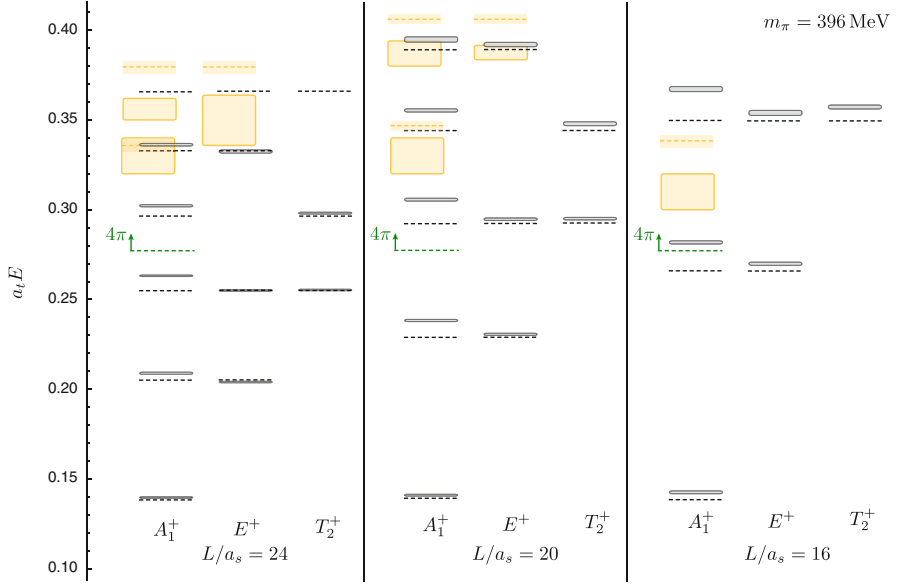


**Fig. 2.13** Energy shifts in  $I = 2$  for three volumes and three lattice irreps. Solid black lines are the energy levels extracted from a variational analysis. The dashed lines are the expected non-interacting levels and the orange boxes are possible  $\pi\pi^*$  scattering states

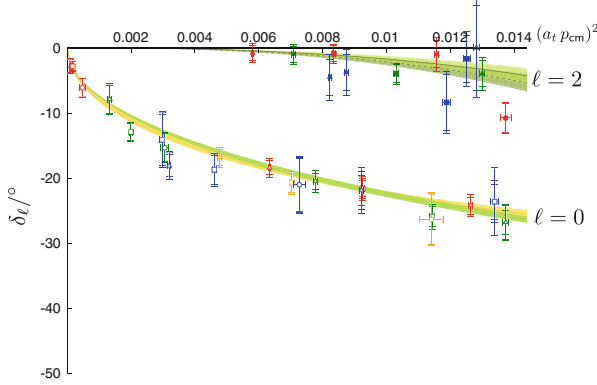


**Fig. 2.14** The phase shift in  $I = 2$ , for  $l = 0$  and  $l = 2$  at a pion mass of 396 MeV

near future and new theoretical frameworks in scattering [130] hint at interesting prospects for further results.



## 2.6 Summary

There is much exciting work in spectroscopy that I have been unable to cover in these lectures and I refer the reader to the proceedings of recent Lattice conferences for further details. I chose to focus on methods, both old and new, for the basic building blocks of spectroscopy and hopefully described their applications as well as some of the attendant pitfalls. Lattice hadron spectroscopy is progressing rapidly at the moment and new ground-breaking calculations and methods are emerging. We can also expect many new discoveries and data for existing and planned experiments in the next ten years. The challenge is for lattice calculations to keep pace!

**Acknowledgements** I would like to thank the organisers for an enjoyable and stimulating school and the INT for support for my visit. I have also been supported by the Science Foundation Ireland through the award of grant number 11-RFP.1-PHY-3201 and by the Research Executive Agency (REA) of the European Union under Grant Agreement number PITN-GA-2009-238353 (ITN STRONGnet).

Lattice QCD for Nuclear Physics

Lin, H.-W.; Meyer, H.B. (Eds.)

2015, XIII, 244 p. 78 illus., 59 illus. in color., Softcover

ISBN: 978-3-319-08021-5